TASK QUARTERLY 10 No 1, 63–81

NUMERICAL MODELLING OF A MULTI-PHYSICAL PROBLEM WITHIN AN ENCAPSULATED THREE-PHASE TRANSFORMER AND ITS SURROUNDINGS

JACEK SMOLKA[1], ANDRZEJ J. NOWAK[1],
DEREK B. INGHAM[2] AND LIONEL ELLIOTT[2]

[1] *Institute of Thermal Technology, Silesian University of Technology, Konarskiego 22, 44-100 Gliwice, Poland*
{*smolka, nowak*}*@itc.polsl.pl*

[2] *School of Mathematics, CFD Centre, University of Leeds, Leeds LS2 9JT, United Kingdom*
{*amt6dbi, lionel*}*@maths.leeds.ac.uk*

(Received 27 January 2006; revised manuscript received 15 February 2006)

Abstract: The paper presents a numerical thermal model of an encapsulated three-phase electrical transformer. The model is based on the multi-physical approach and involves heat transfer analysis coupled with the examination of specific power losses in the coils and the core using electromagnetic field analysis as well as determination of thermal stresses. The thermal boundary conditions (*i.e.* local heat fluxes) are determined by considering a numerical model of the surrounding air. Additionally, the device is cooled via radiation (from the external walls) and forced convection (a water cooling system). A few different configurations of the cooler and the heat pipes are also analyzed. Moreover, anisotropic material properties were applied for stranded coils and the core. A partial experimental validation of the model has shown that the temperature distribution within the transformer is more realistic and closer to the measurements when compared with the previous analysis limited to heat transfer problems only with uniform internal heat sources and isotropic material properties. The total heat transfer rate indicates that forced convection is the most important heat dissipation mechanism in this model. The significance of the water cooling system has also been established in calculations of crack presence in the model.

Keywords: numerical modelling, electrical transformer, local heat sources, heat generation, coupled problem, anisotropic material properties

1. Introduction

Electrical transformers are nowadays commonly used to supply electricity to many industrial machines. In many situations, electrical transformers have to operate under quite rigorous conditions. For instance, many strict conditions need to be fulfilled in a mining environment, where all devices must be fire resistant and

impervious to high humidity. Therefore, the transformer considered in this study is encapsulated in a metal container filled with polymerized resin. Applications of this method are widely used in modern industry, as it offers appropriate fire and ground water protection [1, 2], but they may render transformers less efficient at heat dissipation and the temperature-rise limit of winding insulation may be exceeded. Hence, to achieve an acceptable working temperature inside the windings, the devices have to be cooled not only by means of natural convection and radiation, but also with forced convection. The analysed transformer is equipped with a water cooling system attached to one of the external walls of the container. Such a cooler consists of a steel cooling coil dipped into an aluminium block. The existing device is connected to the bottom wall of the transformer casing. However, other configurations of the cooling system have been also analysed in this project, *viz.* the device located on top or two coolers working together (one on top and the other at the bottom of the transformer casing). Additionally, the heat dissipation process has been enhanced by means of water-copper heat pipes, which connected either the core or the coils with the cooling system. Moreover, the influence of various thicknesses of the lower transformer mountings on the maximum winding temperature has been examined.

The considered transformer dissipates heat from its external walls to the environment by natural convection and to the internal walls of the laboratory - by radiation. In an earlier project (see [3]) the prescribed convective boundary conditions utilized average Nusselt numbers on particular walls, an approach commonly found in the literature [4, 5]. Other authors [6, 7] proposed a more accurate definition of the boundary conditions. In [7] convective heat transfer coefficients are functions of wall temperature, while in [6] the temperature-dependence of both convective and radiative heat transfer coefficients are taken into account. However, this dependence is still based on the average wall/boundary temperature. A more realistic model has been developed in this paper, which includes fluid flows (*i.e.* the air surrounding the transformer itself and the cooler). This means that the model allows us to determine local and temperature-dependent heat fluxes (both convective and radiative) on the transformer's external walls. In order to perform such calculations, continuity of the temperature and heat flux at the interface between the transformer and the surrounding air is enforced through an iterative procedure.

In such devices, the heat is mostly generated within the coils and many authors (*e.g.* see [8]) consider these losses as the only transformer losses. Since heat generation in the coils is the dominant transformer loss, in many applications this simplification is adequate. However, in the present project the specific power losses from the core were meaningful and they have also been taken into account while analyzing the impact of all the main losses on the final temperature field. If all the operating electrical parameters and material properties of the three-phase YY transformer are known, the volumetric heat sources generated within the windings and the core can be calculated and/or measured based on the procedures described in the literature [9]. However, these procedures typically assume that heat is generated uniformly within the whole volume of a particular transformer element [10]. This approach was also followed in our previous work [11], where a numerical model of a transformer involves heat transfer processes only. The total power losses in the coils and core (expressed in

Watts) were known from electrical measurements in short-circuit and open-circuit tests, respectively [9].

Calculations of the coil loss, known as Joule heat, are well documented in the literature [9, 12]. They are usually determined on the basis of local current flux and temperature-dependent electrical resistivity, which requires a coupling procedure [7]. In the case of core losses, the transformer literature also reports a large number of calculation algorithms (see *e.g.* [13, 14]). A typical approach to sinusoidal excitation currents and low frequencies is application of a Steinmetz-based equation [15–18]. This method can be applied to obtain locally the total specific power losses within the core, if the amplitude of the magnetic flux field is known. Therefore, to obtain a more reliable and accurate power loss distribution, in this research thermal/CFD analysis (performed using the Fluent CFD package [19]) is coupled with an analysis of the electromagnetic field (performed using the EMAG module of the Ansys FEM package [20]) through an iterative procedure [6, 7].

Due to the complicated, heterogeneous construction of the transformer coil, attention should be paid to its proper and accurate modelling in terms of thermal properties. In [21] an analysis of the theoretical determination of anisotropic effective thermal conductivities was performed for typical winding configurations, while the authors of [22] presented a numerical model for the effective thermal conductivities of high-T_c superconducting coils. In our previous project [23], the values of the thermal material properties of the coils and the core were decreased and retained isotropic, while in this project these quantities were considered as anisotropic. The core consists of laminates and its thermal conductivity across the laminates is different than that along them. Similarly, the thermal conductivity of the coils is much higher along the wires than in their cross-sectional plane. Analytical models have been used to determine the effective values of the properties for the core (in each direction) and the coils along the wires. However, for both directions in the plane cross-sectional to the wires, these values were obtained numerically. The material properties of other model elements were assumed to be isotropic.

Since a few cracks were observed in the real transformer between the resin and metal elements of the transformer casing, the coupled analysis of the considered transformer was also completed with a determination of thermal stress. An estimate of the level and location of stress was required for safety reasons. The calculations were carried out using the Nastran package and utilizing the final temperature field obtained in the CFD solution. The final part of the project consisted in an analysis of the cracks' impact on the maximum temperature in the windings. Both actual and hypothetically possible cracks were simulated.

2. Geometry and discretisation

All geometrical models and meshes were generated with Gambit (Fluent pre-processor). In the CFD part of the project, the computational domain consisted of two main subregions. The first one included the transformer and the lower or upper cooler. All the device's elements, such as the coils, the core, the transformer base, coil insulation and core mountings were kept in their original shapes and dimensions. The transformer was placed into the casing, which had the dimensions of

0.233 m × 0.146 m × 0.1525 m, and filled with polymerized resin (see Figures 1 and 2). The water cooling system consisted of a steel cooling coil dipped in an aluminium block (0.250 m × 0.170 m × 0.035 m). Three different configurations of the cooler were analysed, *viz.* a single device attached to the bottom wall (see Figures 1a and 1b) or to the top wall, and two coolers working simultaneously (one attached to the bottom wall and the other to the top wall of the transformer casing). A few types of grids were generated within this geometry, following which the impact of the mesh-size on the final results was analysed. Eventually, a hexahedronal mesh with more than 320 000 elements was used for most of the tests. The other subregion consisted of the surrounding calm ambient air and, in the case of the transformer with two coolers, the upper cooling system. The temperature and velocity values at the boundary showed that the external dimensions (2.233 m × 2.146 m × 1.1705 m) of this submodel were large enough to produce size-independent final calculation results. This subdomain was considered in orderto analyse in detail the heat dissipation process controlled by natural convection in the environment. The final mesh of the model of the surrounding air consisted of 250 000 hexahedral elements.

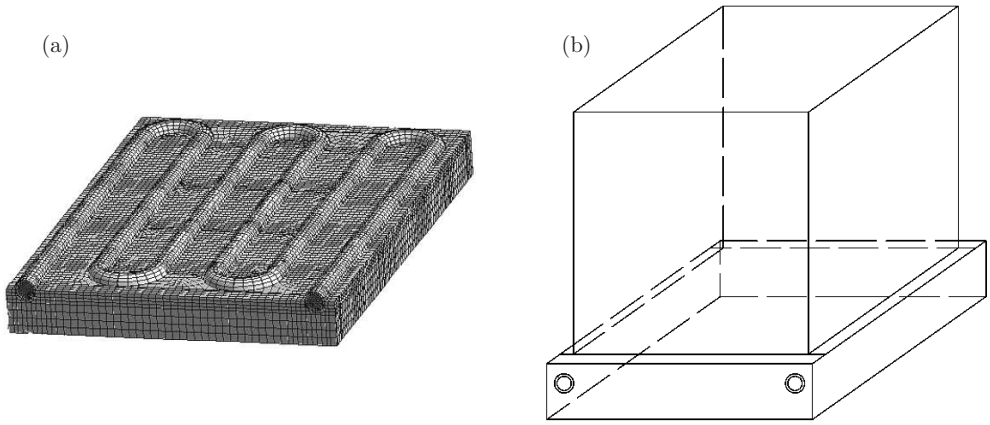

Figure 1. (a) Geometrical model of the lower half of the cooler; (b) the transformer casing with the cooling system

The interfaces between the above defined subregions were the external walls of the transformer casing and its cooling system. It is important to mention that the mesh generated on these surfaces was different for each subregion, since the submodels were built and analysed separately in the iterative procedure. Hence, it was not necessary to generate a very fine mesh for the surrounding air and the total number of elements in the two separate meshes was smaller than it would have been in a single model of the transformer, cooler and surrounding air. Obviously, it reduced the computational expenses.

3. Mathematical model

The temperature distribution in the device and its surroundings can be determined by solving the following energy equation [24]:

$$\nabla(k\nabla T) + q_v = \rho c \boldsymbol{w} \cdot \nabla T, \tag{1}$$

where k is thermal conductivity, T represents temperature, q_v stands for the volumetric heat source, ρ is density, c is the specific heat and $\boldsymbol{w}$ stands for the velocity vector.

The internal volumetric heat sources, q_v, occuring in Equation (1) are the results of electromagnetic analysis. Details of the coupling of the electromagnetic field with the main CFD model are given in the following subsection.

For fluids, *viz.* the water and air considered in this analysis, the energy equation (Equation (1)) should be supplemented with the continuity and momentum equations. The steady state continuity equation for incompressible fluids may be given as follows (*cf. e.g.* [25]):

$$\nabla \cdot \boldsymbol{w} = 0, \tag{2}$$

while the momentum equation can be expressed as follows (*cf.* [25]):

$$\rho \boldsymbol{w} \cdot \nabla \boldsymbol{w} = \boldsymbol{F} - \nabla p + \mu \nabla^2 \boldsymbol{w}, \tag{3}$$

where $\boldsymbol{F}$ stands for the body force vector, p represents pressure, and μ is the dynamic viscosity.

The following additional models were employed in the CFD analysis:

- the incompressible ideal gas law for the density variations in the surrounding air (this relationship is typically designed for natural convection problems),
- the standard k-ε model for the turbulence within the water cooling system ($\mathrm{Re} = 4500$).

3.1. Local volumetric heat sources – coupling with the electromagnetic field

An analysis of the electromagnetic field was performed in Ansys (EMAG module) to compute local volumetric heat sources within the device. The considered transformer was a three-phase YY device operating under the following parameters: PRI – $U = 3 \times 380\,\mathrm{V}$, $f = 50\,\mathrm{Hz}$, SEC – $U = 3 \times 42\,\mathrm{V}$, $I = 13.8\,\mathrm{A}$, $P = 1000\,\mathrm{VA}$. In order to supply power to the device, a three-phase electric circuit was created. The circuit consisted of three independent voltage sources (IVS), three resistors (R), three internal resistors (IR) and six 3D stranded coils (SC). Such configuration of the circuit is very universal because the independent voltage sources can be used to set arbitrary phase voltages and angles. Additionally, different values of electric resistance in the secondary circuit elements enable transformer simulations under various power conditions, *viz.* short-circuit, open-circuit test and rated parameters. Most test cases were performed for the transformer operating under nominal parameters, *i.e.* with resistance of the resistors in the secondary circuit set at $3\,\Omega$.

The geometrical model was originally the same as that used for the thermal calculations. However, the mesh sensitivity analysis performed for this case allowed a reduction of the maximum node number. Eventually, a hybrid grid consisting of almost 52 000 elements was used. Then, after the mesh generation process, the three-phase circuit was coupled with the 3D geometrical model of the transformer (see Figure 2).

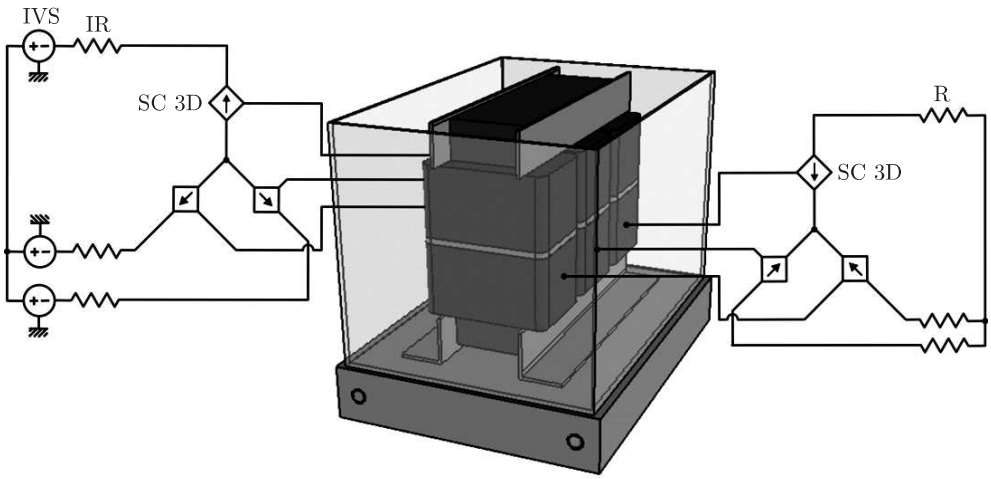

Figure 2. Electric circuit for the electromagnetic calculations: IVS – independent voltage source, IR – internal resistance, SC 3D – stranded coil, R – resistance

The following steady-state Maxwell's equations [12] needed to be solved in order to obtain a solution of the coupled electromagnetic field:

$$\nabla \times \boldsymbol{H} = \boldsymbol{J}, \tag{4}$$

$$\nabla \times \boldsymbol{E} = \boldsymbol{0}, \tag{5}$$

$$\nabla \cdot \boldsymbol{B} = \boldsymbol{0}, \tag{6}$$

where $\boldsymbol{H}$ was the magnetic field vector, $\boldsymbol{J}$ represented the current density vector, $\boldsymbol{E}$ was the electric field vector, and $\boldsymbol{B}$ stood for the magnetic flux vector.

The above set of equations can be solved by means of the magnetic vector potential approach. This method has been successfully applied to transformer-related problems [26] subject to the appropriate boundary conditions being introduced. In this study the boundary conditions of the first kind (Dirichlet) were prescribed on all the external walls of the model,

$$A(x,y,z)|_s = A_s, \tag{7}$$

where A_s is the value of the particular component of the magnetic vector potential at the boundary. During all electromagnetic simulations, the component of the magnetic vector potential, A_s, was explicitly set at zero. This means that the magnetic flux was parallel to each boundary, S, of the considered domain.

The above equations and boundary conditions had to be completed with adequate electromagnetic material properties. Values of the electric resistivity of the windings and the magnetic relative permeability of the core were $1.8 \cdot 10^{-8}\,\Omega$m and 2000, respectively. Most of the simulations were based on these values. However, a sensitivity analysis of relative permeability was also carried out for the core and then the property varied from 1500 to 2500.

The temperature-dependent resistivity required coupling of electromagnetic and CFD solutions through an iteration process. Namely, the heterogeneous temperature field in the coils was used to define a new set of local magnetic properties for the core to be applied in the electromagnetic model. Then, an electromagnetic simulation allowed

us to determine the local heat losses in the windings (the Joule losses) according to the following formula:

$$\boldsymbol{q_v} = \frac{1}{2}|\boldsymbol{J}|^2 \cdot \rho_c, \tag{8}$$

where ρ_c is the electrical resistivity of the windings.

Calculations of the transformer core energy losses required two steps: (i) Ansys EMAG produced a magnetic flux field in each mesh element of the core and (ii) these values were used to produce a curve of the specific power loss in $\mathrm{W/m^3}$ as a function of the maximum magnetic flux and frequency [15]. This procedure produced the following equation:

$$q_v = m \cdot f \cdot B_{max}^n, \tag{9}$$

where f was the frequency and B_{max} stood for the maximum magnetic flux, m represented a coefficient equal to 0.061, the value of exponent n, as usually referenced in literature [27], was equal to 2.5. Coefficient m depended on a number of quantities, *e.g.* core geometry. Its final value was determined on the basis of calculations and experiments. Since the total core loss was obtained from open-circuit experimental tests, its value and the value of the core volume were used to specify the coefficient by summation of all the local losses according to Equation (9).

All the volumetric heat sources calculated with Ansys EMAG were interpolated and implemented into the finer mesh in the Fluent solver (with User Defined Functions).

3.2. Local boundary conditions

In order to determine the temperature distribution in the transformer and the surrounding air, it was necessary to complete the above equations with appropriate boundary conditions and material properties. The thermal model consisted of two separate submodels, namely the transformer with the cooling system and the surrounding air. Hence, two different sets of boundary conditions were required as follows.

(a) External boundary conditions of the surrounding air

- Pressure outlet boundary conditions were prescribed on all the external walls of the surrounding air. This is a typical boundary condition type for flows that can reverse direction near a boundary, which requires specification of the static pressure and temperature of 'backflow' at the outlet boundary. Since all the reported calculations refer to experiments performed in the laboratory, these parameters were set at 101 325 Pa and 292 K, respectively. All other flow quantities were extrapolated from the interior values.
- Parameters of the flowing water at the inlet were set at the temperature of 286 K and the velocity of 0.66 m/s.

(b) Internal boundary conditions at the transformer-air interface

Standard continuity boundary conditions were prescribed along each interface of the problem, including the interface between the transformer and the surrounding air, *i.e.* the temperature and the heat flux had to be the same on both sides of the interface. However, it was noticed during the thermal measurements that contact between the aluminium cooler and the steel container was not perfect, and a thermal contact resistance occurred between these two surfaces. In numerous tests the resistance of

a thin layer of air (of 0.1 mm) was taken into account by determining an equivalent thermal conductivity in the z direction for the bottom wall of the steel container. This value was used as a tuning parameter for the model: its sensitivity was discussed in [3].

The continuity conditions at the interface between the two subdomains, namely the transformer and the surrounding air, were enforced through an iteration process. This process can be summarized as follows: the starting boundary heat flux profile was calculated with the average heat transfer coefficient as discussed in [11]. The obtained temperature profile was then prescribed to the subregion of the surrounding air. Fluent analysis of the air subregion provided a convective heat flux boundary profile in the air, while the radiative heat flux was calculated in the standard manner on the basis of heat exchanged between transformer, the cooler and the environment [24]. Temperatures utilised in these formulae were those of the external transformer and the cooling system's walls as well as the internal walls of the laboratory. The sum of convective and radiative heat flux was then prescribed back to the transformer subdomain. The next step was to recalculate the interface temperature by analysing the transformer. This iteration process was continued until the temperature and heat flux profiles in two subsequent steps were sufficiently close. The convergence criteria employed in this paper involve δ_T and δ_q errors, which should not exceed 0.001%. These errors are defined as follows:

$$\delta_T = \frac{|\overline{T_i} - \overline{T_{i+1}}|}{\overline{T_i}} \cdot 100\%, \tag{10}$$

$$\delta_q = \frac{|\overline{q_i} - \overline{q_{i+1}}|}{\overline{q_i}} \cdot 100\%, \tag{11}$$

where δ_T is the temperature error, $\overline{T_i}$ and $\overline{T_{i+1}}$ are average temperatures in two consecutive iteration steps, δ_q stands for the heat flux error, while $\overline{q_i}$, $\overline{q_{i+1}}$ represent average heat fluxes in two consecutive iteration steps. The average temperatures and heat fluxes of the container top wall (the hottest surface) were used in these formulae.

When the transformer with two coolers was considered, one subdomain consisted of the transformer and the bottom cooler, while the other included the surrounding air and the top cooler. However, this test required the use of underrelaxation to obtain convergence. The iterative procedure applied in this project was as follows [28]:

$$q_{i+1}^{trans} = (1-\omega) \cdot q_i^{trans} + \omega \cdot (-q_i^{air}), \tag{12}$$

where q_i^{trans} was the total heat flux prescribed to the boundaries of the transformer and the bottom cooler subdomain in the previous iteration, q_i^{air} was the total heat flux produced by the surrounding air and the top cooler subdomain in the previous iteration, and ω was the underrelaxation factor. The value of the underrelaxation factor was determined empirically. During a few initial iterations it was set to 0.0001 and was subsequently increased to 0.005.

3.3. Anisotropic thermal material properties

In our previous project [11] simplified modelling of material properties was used and the values were defined as isotropic both for the coil, and the core. However, in the current project anisotropic material properties were defined for these elements

due to their specific construction, anisotropic material properties for these elements were defined. As the results show, this procedure appears to be much more accurate. A typical coil consists of wires, wire insulation, air filling the gaps between the wires, and insulating tape covering the external layer of wires in each coil (see Figure 3c). It has been assumed in this study that both the coils and the core behave like a homogenous material and have only one equivalent (effective) value [22] of thermal conductivity in each direction of the coordinate system.

(a) Effective thermal conductivity for coils: In order to determine the equivalent thermal properties of a coil, three geometrical regions had to be distinguished: corners and two straight, perpendicular parts of the coil (see Figure 3a). The same three thermal conductivities k_i, k_j, k_k were specified in these subregions, but their values were applied for different directions and/or coordinate systems. Namely, a Cartesian coordinate system was defined in the straight parts (four regions), while cylindrical coordinates were employed in the corners (also four regions, see Figure 3a). Moreover, the effective values of thermal conductivity were determined in two different ways: a numerical conduction model was used for the two directions cross-sectional to the wires [21, 22], while an analytical model was used for the direction along the wires.

In order to determine anisotropic thermal conductivities for the direction cross-sectional to the wires, a 2D *numerical model* of the coils' cross-section was developed (see Figure 3b). However, taking into account different values of wire diameter and the wire insulation thickness in the primary and secondary windings, two separate geometrical models were created. The geometrical model of the primary coils consisted of 428 turns, while that of the secondary coils had 50 turns only. Apart from copper wire, the insulating tape, the wire insulation and the air between the wires were also modelled and these component conductors were considered as isotropic. A part of the mesh applied in the model for the secondary coils is shown in Figure 3c.

For each type of coils, two tests were carried out in order to determine their thermal conductivities in two perpendicular directions. In the 2D models, conduction occurred in the wires and in the insulation materials, while natural convection and radiation were considered in the air gaps. Hence, to calculate the effective thermal conductivity in the vertical direction, the boundary conditions in the numerical model (see Figure 3b) were prescribed as follows: two vertical parallel walls were insulated (no heat flux through the boundary), while the Dirichlet (known temperature) and Neumann (known heat flux) boundary conditions were specified on the other parallel horizontal walls. It turned out that the values of temperature and heat flux could be chosen arbitrarily since the influence of convection and radiation occuring in the air gaps was negligible.

From the above-discussed calculations the average wall temperature was obtained at the surface where the heat flux was prescribed. Subsequantly, the effective thermal conductivity in the i^{th} direction (y^{th} in Figure 3a) was computed from the following equation (the Fourier law) [12]:

$$q_i = -k_{i,eff}\,\frac{\partial T}{\partial i}, \tag{13}$$

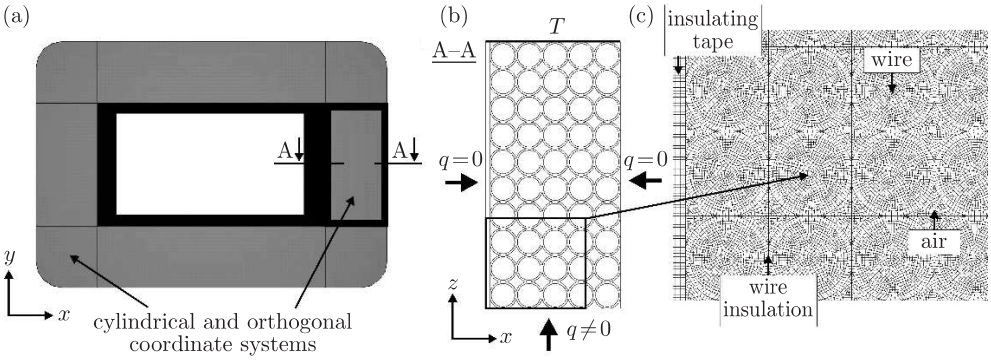

Figure 3. Geometry: (a) coils; (b) their cross-sectional 2D model; (c) a part of the model's mesh

where q_i was the heat flux in the i^{th} direction and $k_{i,eff}$ – the effective thermal conductivity in the i^{th} direction.

Analytical models were utilised in the case of thermal conductivity in the direction along the wires. Namely, an analogy of electrical resistivities connected in a parallel circuit was used to compute the effective value of this property. Therefore, the following relationship could be used for the i^{th} direction:

$$k_{i,eff} = L_i \cdot \sum_{j=1}^{n} \frac{k_j}{L_j}, \tag{14}$$

where L_i stood for coil length in the i^{th} direction, k_j was the thermal conductivity of the j^{th} material of the coil, while L_j represented the length of the j^{th} material layer of the coil in the i^{th} direction.

(b) Effective thermal conductivity for the core: The considered core consisted of flat steel laminates separated from each other by a layer of varnish. Hence, in the case of the core, thermal conductivity was computed in each direction using analytical models. Its effective value was considered as a connection of the parallel resistivities for the two directions parallel to laminates (see Equation (14) above), while the following formula for a connection of serial resistivities was used for the direction perpendicular to the laminates:

$$k_{i,eff} = \frac{L_i}{\sum_{j=1}^{n} \frac{k_j}{L_j}}. \tag{15}$$

The thermal properties of the solids in the transformer were generally gathered from the standard literature and their suppliers and were set at: 391 W/(mK) for copper, 171 W/(mK) for aluminium, 1.04 W/(mK) for resin and 35 W/(mK) for carbon steel. Taking these into account, the following values of effective thermal conductivity were obtained for the coils: $k_x = k_z = k_r = 1.0\,\text{W/(mK)}$, $k_y = k_\phi = 231.5\,\text{W/(mK)}$, with $k_x = k_z = 34.4\,\text{W/(mK)}$, $k_y = 15.1\,\text{W/(mK)}$ for the core.

4. Modelling of heat pipes

In this project heat pipes were considered as super-conductive solids [29]. In the temperature range relevant to the transformer, the most suitable heat pipes are water-copper and methanol-copper ones, both with sintered wicks. Typically,

the effective thermal conductivity of this type of heat pipes is in the range of $k = (50–250)\,\mathrm{kW/(mK)}$. During most of our tests performed with heat pipes, the effective thermal conductivity in the direction along the pipe was set at $k = 50\,\mathrm{kW/(mK)}$. In this project, the heat sources loading the heat pipes were the core and the coils, whereas the heat sink was a water cooling system. It was assumed that the hot end of the heat pipe was soldered to the transformer core or attached to the coils with resin, while the cold end was soldered to the bottom wall of the casing connected directly to the cooling system. Several configurations of heat pipes were considered. In one of the tests, ten heat pipes were attached to the right- and left-hand sides of the core, both below and above the coils (4×10 pipes in total, see Figure 4).

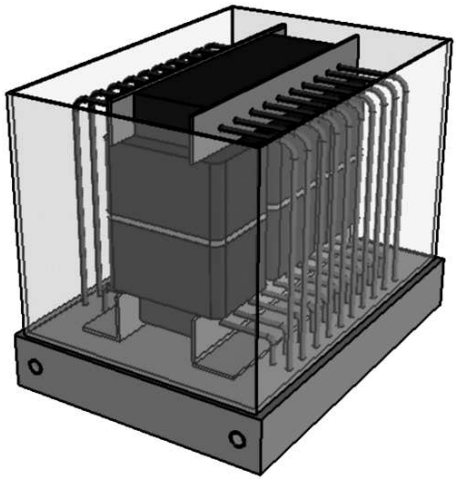

Figure 4. Sample configuration of heat pipes

However, all the analysed cases described ideal devices without any contact resistance. Hence, another series of calculations considered thermal contact resistance as well. $R = 0.5 \cdot 10^{-4}$ $(\mathrm{m^2K})/\mathrm{W}$ was prescribed for the heat pipes attached to the transformer's core and bottom wall of the casing by soldering and $R = 1.0 \cdot 10^{-4}$ $(\mathrm{m^2K})/\mathrm{W}$ – those attached to the coils' external surfaces by means of resin [30].

5. Determination of the stress field based on the final temperature field

In mechanical analysis, thermal stresses are obtained basing on known displacements and strains occuring within a model [31]. These quantities can be determined if appropriate loads and boundary conditions are defined. The only load in this analysis was thermal loading. The temperature field utilized in the thermal stress calculations was obtained from the CFD model as described in the preceding sections. Similarly, the temperatures and the mesh definition were extracted from Fluent and translated into a neutral file format.

During experimental measurements, the transformer with its cooling system was placed on a table in the laboratory. For this reason, the boundary conditions in the model were defined as follows. At the bottom wall of the cooling system, only

translations in the z direction were set to zero. Additionally, in order to fix the model physically, the translations in the x, y and z directions were set to zero for a single node located in the centre of the bottom wall. All other boundaries were made free. The material properties for the resin, such as the Young modulus and the linear expansion coefficient, were provided by the supplier and were set to be temperature-dependent. All other material properties originated from the standard literature.

Once a neutral file was generated and completed with the boundary conditions as well as the material properties, it was used as an input file for the MSC Nastran code.

6. Final temperature field with a crack

Generally, cracks cause a temperature discontinuity, which can lead to significant temperature increases. Hence, it was tested in this project whether or not such an increase could damage the insulation of the transformer windings.

In the tested transformer, cracks occurred in two regions: one – at the interface between the surrounding resin and the core, transformer mounting and coils (see Figure 5a), the other – at the surface between the resin and the model's casing (see Figure 5b). These cracks were simulated as a thermal resistance equivalent to different air layers. Thicknesses of 0.1 mm and 0.5 mm of the air layers were considered.

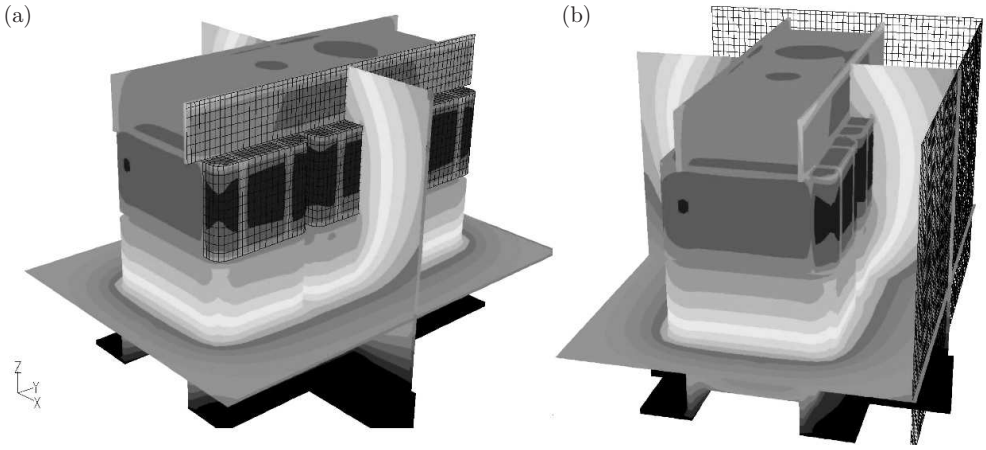

Figure 5. Location of the simulated cracks (meshed surfaces): (a) between the resin and the core, transformer mounting and coils; (b) between the resin and the casing

For a more complete analysis of the cracks' impact on the final temperature field, a few simulations were performed for the case in which the forced cooling system was turned off.

7. Results and discussion

(a) Iterative procedure: As explained above, CFD analysis requires an iteration loop between two submodels: transformer with the cooling system and the surrounding air. A plot of the convergence process as a function of the number of iterations is shown in Figure 6. The error, δ_T^1, of the first loop was determined considering the

temperature profile obtained from the calculations with uniform heat sources and the temperature profile from the first iteration of this project. The first heat flux error, δ_q^1, was determined from the heat flux profile in the air subregion with a prescribed temperature profile from the initial step and that from the subsequent loop. The iteration process appeared to be very efficient, since after nineteen steps the error was less than 0.001%. Since the air submodel required many more iterations to obtain convergence, each step consisted of 20 iterations for the transformer submodel and 60 for air. The number of iterations in a step was set at these values taking into account the time taken to read and write all the case files.

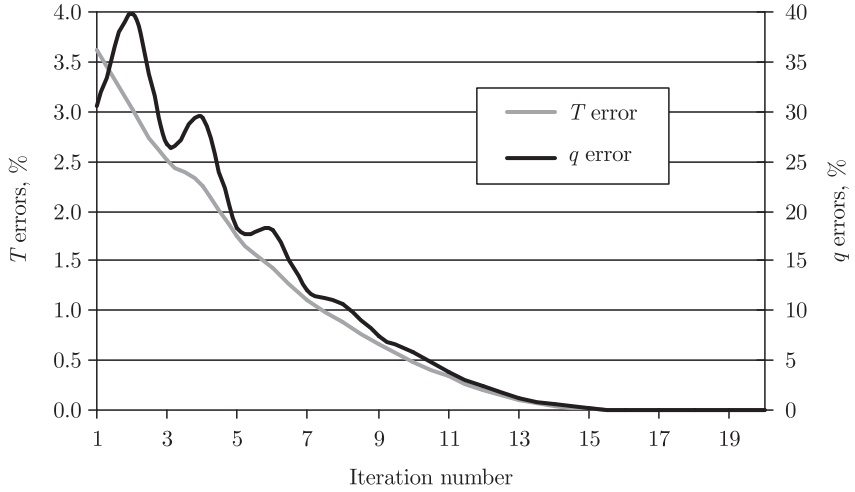

Figure 6. Convergence rate as a function of the number of iterations

In the case of two coolers attached to the bottom and top wall of the transformer casing, many more iterations were required compared with the case of the transformer with single coolers, *viz.* the solution converged after 60 iterations. This can be easily explained by taking into account the location of the interface between two submodels. During these tests, one submodel consisted of the transformer and the bottom cooler, while the other consisted of the surrounding air and the top cooler. This means that on the interface between two solids, *i.e.* the top wall of the transformer casing and the bottom wall of the upper cooler, the latter subdomain produced large heat fluxes. Therefore, very low values of the underrelaxation factor were used.

(b) Local source terms: In [11] values of the internal heat sources originated from measurements. Such an approach resulted in uniform values for these sources within the whole volumes of the coils and core, while in this study electromagnetic analysis enabled determination of their local values. The distribution of magnetic flux in the core (expressed in Teslas, see Figure 7a) was used to calculate source terms for thermal analysis. The values of heat sources implemented in Fluent by means of User Defined Functions varied in the core from 0.012 to 278kW/m^3 (the average was 32.3kW/m^3), and their maximum values occurred around the primary windings (see Figure 7b). The heat source distribution presented in Figure 7b affected the overall temperature field.

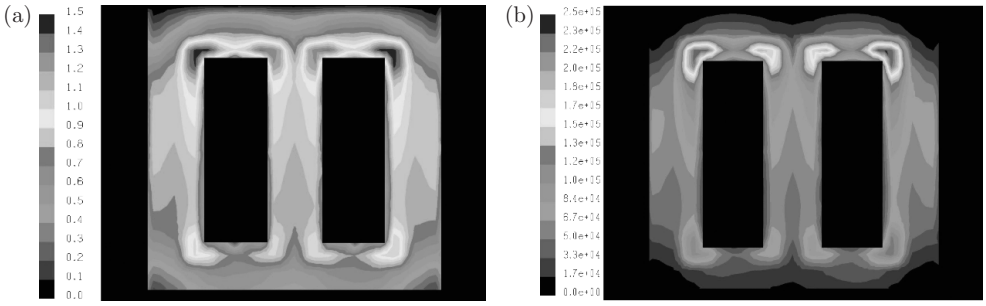

Figure 7. Cross-sectional views of the transformer core: (a) distribution of magnetic induction [T]; (b) internal heat sources [W/m^3]

The temperature values at selected measurement points (see Figure 8) are listed in Table 1. In the first two columns of this table, values of the solution are shown with local internal sources compared to those obtained for uniform sources. As expected, differences in the temperature values in these columns are quite small because of the position of measurement points on the external surfaces of the coils.

(c) Sensitivity of electromagnetic material properties: In columns 2, 2a and 2b of Table 1, results of the sensitivity analysis of the magnetic relative permeability utilized for the core are presented. These results show very small impact of this material property on the final temperature field, which can be explained by taking into account the ratio of heat generated in the core to the total heat losses from the transformer (only 20%).

The values in column 3 of Table 1 indicate that a further slight increase in temperature in the case of temperature-dependent copper resistivity being applied to the coils. This weak temperature dependence can also be concluded from Figure 9a, in which the temperature field is almost uniform.

(d) Additional radiation: The next column of Table 1 presents the results of tests in which, in addition to the convective boundary conditions, radiative ones were considered as well. The influence of radiation is not significant due to a low value of the maximum wall temperature (< 326K). However, the temperature values listed in this and the preceding columns are closer to the experiments than those from column 1. It seems that the influence of local boundary conditions would be more significant for devices cooled by means of free convection only.

(e) Anisotropy of thermal material properties: Significant increases in the temperature field can be observed in column 5 of Table 1. These results were obtained for anisotropic thermal material properties, *i.e.* strong influence of the coils. In this case, the computed effective thermal conductivity in the directions perpendicular to the wires, 1.0W/(mK), was very low compared with the isotropic values, 200W/(mK), used in [11, 23]. The temperature field obtained for this case is presented in a cross-sectional view in Figure 9a, where it can be observed that the greatest temperature gradients occur in the core. Hence, the heat is mostly transferred from the coils to the cooling system through the transformer core.

In the sixth column of the Table, temperatures are listed for the case in which the thermal contact resistance between the transformer casing and its cooler has been

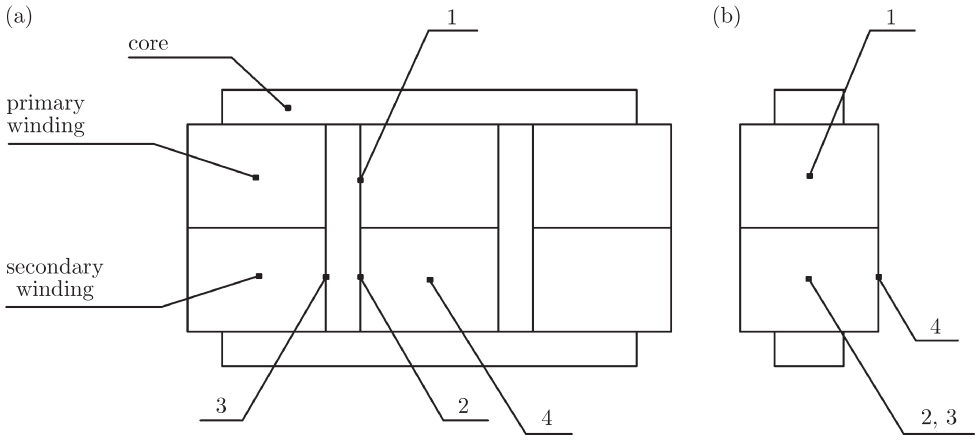

Figure 8. Schematic layout of the thermocouples' (measurement points') location on the transformer coils: (a) main view; (b) side view (temperatures at these points are listed in Table 1)

neglected. The values of the measured temperatures are between those obtained from columns 5 and 6, which means that although the assumed contact resistance of 0.1 mm in the air layer was slightly too high, it still exists and affects the whole temperature field in the transformer.

Table 1. Temperature field in the transformer with the cooling system: column 1 – uniform internal heat sources, local convective BCs, isotropic material properties, contact resistance between transformer casing and cooling system; column 2 – as in 1, but with local internal heat sources ($\mu_r = 2000$ for the core); column 2a – as in 2, but $\mu_r = 1500$ for the core; column 2b – as in 2, but $\mu_r = 2500$ for the core; column 3 – as in 2, but electric resistivity for windings is temperature-dependent; column 4 – as in 3, but local BCs are both convective and radiative; column 5 – as in 4, but thermal properties for the coils and the core are anisotropic; column 6 – as in 5, but contact resistance is neglected; column 7 – as in 1, but a cooler is located on the top casing wall; column 8 – as in 5, but with twelve real heat pipes attached to the upper part of the core; column 9 – as in 5, but the second cooler is attached to the top casing wall (system with two coolers)

Measurement point	Measured temperature [K]	Calculated temperature [K]										
		1	2	2a	2b	3	4	5	6	7	8	9
1	332.0	325.8	326.5	326.4	326.5	326.7	326.2	338.1	329.8	324.0	320.9	309.3
2	332.3	324.5	325.0	325.0	325.0	325.2	324.7	330.3	320.8	325.3	316.1	309.2
3	328.0	324.2	324.9	324.8	324.9	325.1	324.6	329.9	320.9	324.7	316.2	309.4
4	323.3	324.5	325.0	325.0	325.1	325.3	324.7	330.1	320.6	325.5	315.9	308.7

(f) Varied thickness of the mountings: As heat travelled through the core and then through the bottom mounting to the bottom cooler or through the top mounting to the top cooler, the influence of the mounting's thickness on the final temperature field was worth testing. The thickness of the existing elements was 2 mm, and this value was increased to 4 mm and then to 6 mm. As a result, the maximum temperature dropped by about 2K for the thickness of 4 mm and by almost 4K for 6 mm. The total

weight of the device did not increase significantly, while the temperature change was noticeable.

(g) Cooler on top: A change of the cooler's position from the bottom to the top did not cause a great temperature difference (*cf.* columns 1 and 7 of Table 1). Clearly, these values are close to each other and the differences result from the transformer's internal structure and its casing.

(h) Application of heat pipes: Results have shown the usage of heat pipes to be quite efficient. Obviously, the larger the number of applied devices, the lower the temperature obtained inside the casing with the transformer. Twelve heat pipes connected to the upper part of the core or attached to the primary coils guaranteed a much lower level of temperatures (drop by about 25K). However, the temperature field changed significantly when the contact resistance of solder and resin, used for attaching the devices, was taken into account; the cooling process turned out to be less effective (see column 8 of Table 1).

(i) Two coolers: Comparing all the heat transfer mechanisms for the case of the transformer with a single cooler, it can be concluded that an effective forced cooling system plays the most important role in the total heat dissipation process. Namely, 99.5W is removed by forced convection, while mere 10.5W and 2.5W is removed by natural convection and radiation, respectively. Therefore, in order to lower the maximum temperature within the analysed object, the forced dissipation process has to be enhanced. It seems that the cheapest way to do so is to use another cooler on top of the transformer casing: the maximum temperature drop is almost 30K (see column 9 of Table 1). It should be stressed that both cross and parallel water flows in the coolers were analysed and the temperature difference in these solutions was limited to 0.2K. Thus, the system with two coolers working together is very effective and the type of cooler connections is of no importance.

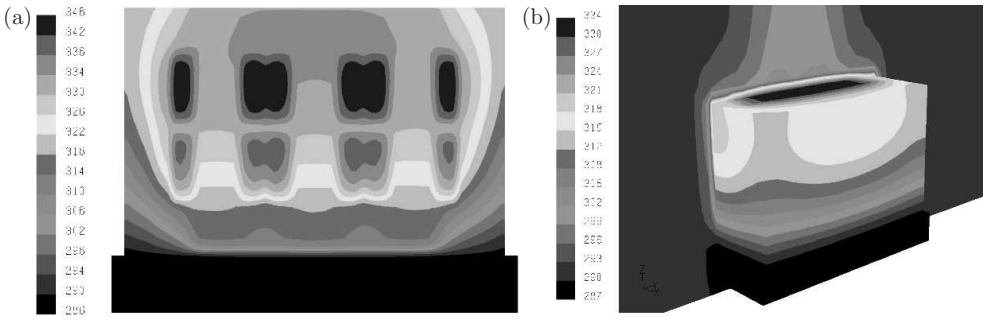

Figure 9. Cross-sectional view of the temperature field: (a) within the transformer; (b) in the surrounding air and on transformer's external walls

(j) Influence of the cracks: The analysis of thermal stresses within the transformer indicates that their highest values occur in the casing's corners. This can easily be explained taking into account the sharp edges of the transformer casing and the differences in the thermal expansion coefficients of steel and resin. Lower levels of stress have been observed on the casing-resin interface, *e.g.* a YY component of the

stress tensor has reached a value of 40MPa. But even this value might be dangerous for the device as the maximum tensile strength for the resin is only 5MPa.

Several tests were carried out to simulate a crack and find out its influence on the maximum temperature of the model. During these calculations different thicknesses of the air cracks were taken into account. Results obtained for the thermal resistance of $0.019\mathrm{m}^2\mathrm{K/W}$ (equivalent to a 0.5mm air crack) showed that the maximum temperature increased by about $\Delta T = 2\mathrm{K}$, compared with the case without any cracks.

Calculations of the transformer's operation, with and without air cracks, have also been carried out for the forced cooling system turned off. Results have shown that the temperature increase in the transformer with cracks, cooled with atmospheric air only is merely $\Delta T = 2.5\mathrm{K}$ when compared with the model without cracks. This proves that heat is exchanged mainly through the core and confirms the importance of the water cooling system.

Apart from the locations described above, thermal stresses obtained in the model have rather small values, even in the regions of the coils and the core. Hence, it appears that thermal stresses would rather not initiate cracks in these locations.

8. Conclusions

Heat transfer problems in an encapsulated electrical three-phase transformer have been presented. One of the aims of this research has been to determine the local heat sources in the transformer's windings and core. It was therefore necessary to carry out an electromagnetic analysis based on experimental data and couple this solution with a CFD simulation. In the main analysis the transformer was cooled using natural convection (in ambient air), radiation (to the internal walls of the laboratory) and forced convection (from the water cooling system attached to the bottom wall). A model of the surrounding air was considered in the analysis of the natural convection problem around the transformer. Two separate submodels, *i.e.* the transformer with the cooler (bottom or top one) and the surrounding air (and the top cooler) were then solved iteratively.

The procedure of modelling an electromagnetic transformer operating in different regimes and coupling the obtained solution with a thermal solution turned out to be effective in terms of the convergence process. The final solution of the study was compared with prior calculations, in which heat sources were assumed to be uniformly distributed, and with measurements of the temperature field in the transformer. The temperature distribution in the transformer was more realistic and closer to the measurements when compared to the case with isotropic material properties. The total heat transfer rate indicates that forced convection is the most important heat dissipation mechanism in the model. Hence, the safe temperature level will be kept inside the windings when an effective forced cooling system is applied. Therefore, various configurations of the existing cooler were analysed, *i.e.* the device located at the bottom, on top or two coolers working together. Additionally, a few tests were carried out using heat pipes to enhance the heat dissipation process. The significance of the water cooling system was also established in calculations of a crack present in the model.

Acknowledgements

The financial assistance of the Polish State Committee for Scientific Research under grant number 3 T11F 022 27 is gratefully acknowledged herewith. The first author is also grateful for the assistance on this project of the Marie Curie Training Site Fellowship at the CFD Centre of the University of Leeds.

References

[1] Altman G and Pfeiffer R 1984 *Siemens Power Engng.* **6** 20

[2] Le Roy G and Sandoz F 1985 *Proc. 8th Int. Conf. on Electricity Distribution, (CIRED)*, UK, pp. 71–76

[3] Smolka J 2001 *Thermal Process Analysis in an Electrical Transformer Dipped into Polymerized Resin*, MSc Thesis, Silesian University of Technology, Gliwice, Poland, and Brunel University, Uxbridge, UK

[4] Eckholz K, Knorr W, Schafer W, Feser K and Cardillo E 2004 *Proc. Cigre 2004 Session*, Paris, France, CD-ROM, paper A2-107

[5] Chang H-M, Choi Y S, Sciver van S W and Choi K D 2003 *Cryogenics* **43** 589

[6] Lefevre A, Miegeville L, Fouladgar J and Olivier G 2005 *IEEE Trans. on Magnetics* **30** 1564

[7] Biro O, Preis K and Buchgraber G 2005 *Proc. Int. Conf. on Computational Methods for Coupled Problems in Science and Engineering Coupled Problems*, Santorini, Greece, CD-ROM, Abstract Book p. 107

[8] Garcia A, Espinosa-Paredes G and Hernandes I 2002 *Computers and Electrical Engng.* **28** 417

[9] McLyman C 1998 *Magnetic Core Selection for Transformers and Inductors*, Marcel Deckker, New York

[10] Radakovic Z and Maksimovic S 2002 *Electrical Engng.* **84** 109

[11] Smolka J, Nowak A J and Wróbel L C 2003 *Computers and Fluids* **33** 859

[12] Rao N N 1994 *Elements of Engineering Electromagnetics*, Prentice Hall, New Yersey

[13] Basak A, Yu C -H and Lloyd G 1994 *IEEE Trans. on Magnetics* **30** 3725

[14] Venkatachalam K, Sullivan C R, Abdallah T and Tacca H 2002 *Proc. 8th IEEE Workshop on Computers in Power Electronics, COMPEL 2002*, Mayaguez, Puerto Rico, CD-ROM

[15] Snelling E C 1988 *Soft Ferrites, Properties and Applications*, Butterwoths Publishing, Stoneham

[16] Lefebvre L P, Pelletier S and Gelinas C 1997 *J. Magnetism and Magnetic Materials* **176** 93

[17] Mulder S 1995 *Power Conversion and Intelligent Motion* **21** 22

[18] Goel N S, Gerboc J S and Lehtonen J 2000 *Int. Comm. Heat Mass Transfer*, Part A **37** 519

[19] Fluent Inc. Product Documentation, http://www.fluent.com.

[20] Ansys Product Documentation, http://www.ansys.com

[21] Lussier D T, Ormiston R M and Marko R M 2003 *Int. Comm. Heat Mass Transfer* **30** 313

[22] Lehtonen J, Mikkonen R and Paasi J 2000 *Cryogenics* **40** 245

[23] Smolka J, Nowak A J, Stępień M and Grzesik B 2004 *Proc. Conf. on Contemporary Problems of Thermal Engineering*, Ustroń, Poland, pp. 435–442

[24] Ozisik M N 1985 *Heat Transfer. A Basic Approach*, McGraw-Hill, New York

[25] Anderson J D (Jr) 1995 *Computational Fluid Dynamics. The Basics with Applications*, McGraw-Hill, New York

[26] Biro O and Preis L 1989 *IEEE Trans. on Magnetics* **25** 3145

[27] Reinert J, Brockmeyer A and Doncker De R W 2001 *IEEE Trans. on Industry Applications* **37** 1055

[28] Bialecki R A, Ostrowski Z, Kassab A J, Yin Q and Sciubba E 2002 *Engineering Analysis with Boundary Elements* **26** 597

[29] Garner S D and Toth J E, *Heat Pipes: A Practical and Cost Effective Method for Maximizing Heat Sink Effectiveness*, The Thermacore Inc. Website http://www.thermacore.com.

[30] DeHoff R and Grubb K, *Heat Pipes Application Guidelines*, The Thermacore Inc. Website http://www.thermacore.com.

[31] Cook R D 1995 *Finite Element Modeling for Stress Analysis*, J Wiley and Sons, New York